Journal of Applied Mechanics and Technical Physics, Vol. 44, No. 6, pp. 770–778, 2003

EFFECT OF PROCESSES AT THE COMPRESSION PULSE FRONT ON SPALLING STRENGTH OF A MATERIAL AND RESISTANCE TO HIGH-VELOCITY PENETRATION

Yu. I. Meshcheryakov and A. K. Divakov

UDC 539.374

Tests on backward spalling of 38KhN3MFA *structural steel,* D-16 *aluminum alloy,* M-2 *copper,* 02Kh18K9M5-VI *maraging steel,* KhN75VMYu *alloy, beryllium, and other materials show that spalling strength correlates with the threshold of structural instability of a material to compression at the leading edge of the compression pulse. It is shown that the threshold of structural instability to compression obtained in experiments on uniaxial deformation of flat targets determines the strength of resistance to high-velocity penetration in the Alekseevskii–Tate model.*

Key words: *spalling strength, high-velocity impact, structural instability of a material.*

Introduction. Spalling fracture of a material in plane loading waves is known to be a result of interference of unloading waves propagating from free surfaces of the projectile and target inward the target. A certain ratio of the projectile and target thicknesses generates tensile stresses inside the target, which lead to spalling. It is usually assumed that spalling strength is a rather objective characteristic of dynamic tensile strength of the material in a microsecond range of loading [1]. In reality, precompression of the material occurs in passing of the leading edge of the pulse. Before tensile stresses are generated in the spalling zone, dynamic compression reaches a certain critical value, and irreversible structural and strength changes occur in the material. The effect of the processes at the wave front on dynamic strength of the material during spalling and high-velocity penetration is considered in the present work by the example of shock loading of a series of materials.

1. Test Technique and Results. The experiments on shock loading of various materials under conditions of uniaxial strain were performed on a light-gas gun 37 mm in diameter. The targets were shock loaded within the range of projectile velocities of 50–600 m/sec. In all tests, the target and projectile thicknesses were chosen such that backward spalling was obtained. The projectile velocity was determined by measuring the time interval between two signals generated when the projectile crossed two laser beams near the loaded target surface. The measurement error for projectile velocity was smaller than 1%. The velocity of the free surface of flat targets was registered by a high-velocity two-channel interferometer [2]. In addition to the profile of the mean velocity of the free surface $U_{\text{f.s.}}(t)$, the test technique allows one to measure the dependence of the root-mean-square deviation of mass velocity on time $D(t)$. In this approach, the shock-wave front is represented as the averaged motion of the deformed medium with a certain mean velocity $U(t)$, which is accompanied by velocity fluctuations on two or more scales characterized by the velocity dispersion D^2_{ms}.

Figure 1 shows the qualitative configuration of the wave front. According to the classification suggested in [3], mesoscale 1 includes structural elements whose mean size is within 0.1–10.0 μm; the mean size of structural elements of mesoscale 2 is 50–500 μm. According to the classification suggested in [4], mesoscale 2 is called the superstructural scale. It is seen in Fig. 1 that the front of the wave propagating in a heterogeneous medium has a complicated multiscale structure, and individual parts of the front have different velocities. The instantaneous values of velocity at mesoscale 1 are denoted as V_{ms1}, and velocity dispersion at mesoscale 1 is denoted as D_{ms1}. The mean velocity at mesoscale 1 is shows by the dashed curve; for mesoscale 2, this velocity is instantaneous.

Institute of Problems of Mechanical Engineering, Russian Academy of Sciences, St. Petersburg 199178.
Translated from Prikladnaya Mekhanika i Tekhnicheskaya Fizika, Vol. 44, No. 6, pp. 25–34, November–December, 2003. Original article submitted November 18, 2002; revision submitted March 17, 2003.

 0021-8944/03/4406-0770 $25.00

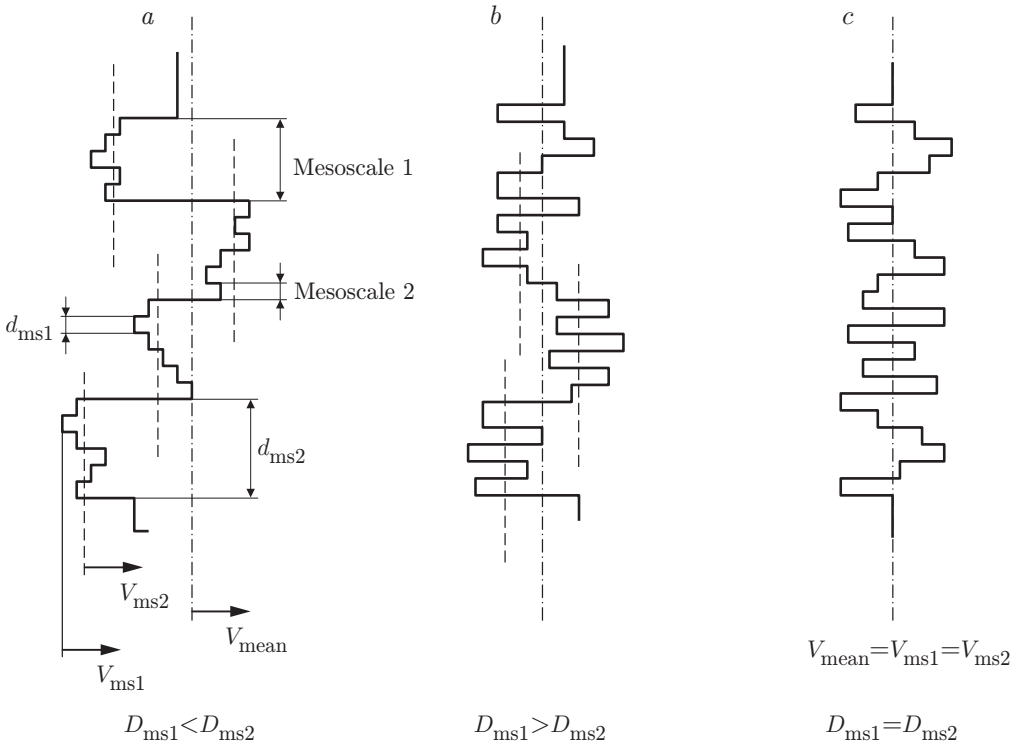

Fig. 1

TABLE 1

Test number	h_t, mm	h_{pr}, mm	U_{pr}, m/sec	U_{max}, m/sec	U_h, m/sec	D, m/sec	W, m/sec	U_A, m/sec
1	5.01	2.0	43.8	40.8	5	0	33.40	35
2	5.00	2.0	61.6	63.2	5	0	48.20	55
3	5.01	1.9	93.9	91.7	4	11.50	49.84	85
4	10.07	1.78	117.0	120.0	4	14.24	60.00	110
5	5.00	1.9	140.4	144.0	4	13.61	60.75	120
6	5.00	1.9	176.6	166.1	4	22.41	62.24	150
7	5.01	1.9	184.1	183.9	5	14.40	69.94	154
8	5.00	1.9	189.0	185.6	4	28.22	58.55	168
9	5.00	1.9	261.0	232.3	5	49.39	59.32	220

The scatter of velocities at mesoscale 2 is characterized by the dispersion D_{ms2}. The dot-and-dashed lines show the mean velocity at mesoscale 2 V_{ms2}, which is also a macroscopic mass velocity of the medium V_{mean}. Such a hierarchy of scales is observed for $D_{ms1} < D_{ms2}$ (Fig. 1a). In the case $D_{ms1} > D_{ms2}$ (Fig. 1b), the mean macroscopic mass velocity of the medium coincides with the mean velocity at mesoscale 1. If the dispersions of mass velocity at the neighboring scales are commensurable (Fig. 1c), the mean velocities at mesoscales 1 and 2 coincide and are considered as the macroscopic mass velocity of the medium.

The test results for M-2 copper are shown in Table 1 (h_t and h_{pr} are the target and projectile thicknesses, U_{pr} is the projectile velocity, U_{max} is the maximum velocity of the free surface on the compression pulse plateau, U_h is the velocity of the free surface on the elastic precursor, D is the root-mean-square deviation of velocity, W is the difference between the maximum value of velocity of the free surface and its value at the rear front at the point of the first reverse of the velocity profile (this quantity is sometimes called the spalling velocity, since it is used to calculate spalling stress $\sigma = 0.5\rho C_0 W$), and U_A is the velocity of the free surface at the leading edge of the pulse at the point where the slope of the front changes drastically before the front becomes a plateau.

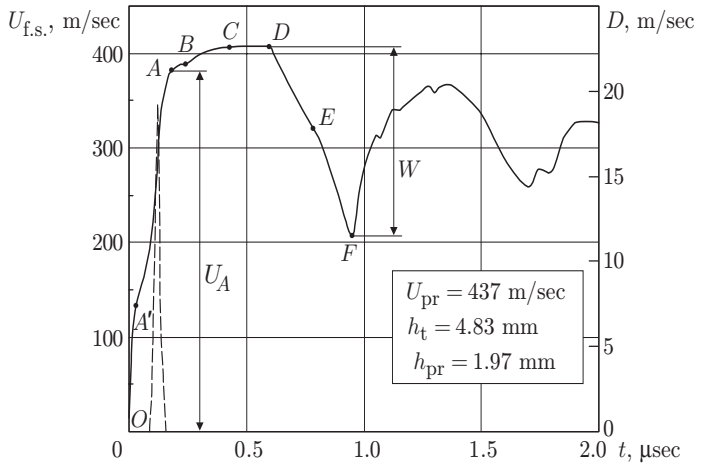

Fig. 2

Figure 2 shows the time evolution of velocity of the free surface of the flat target made of 30KhN4M steel (solid curve) and the root-mean-square deviation of velocity (dashed curve). The free-surface velocity profile measured by the interferometer has several characteristic regions, which are clearly seen in all experiments: elastic precursor (sector OA'), plastic front ($A'A$), transitional region (AB), flat sector of the plastic loading front (BC), plateau of the compression pulse where the free-surface velocity remains constant (CD), elastic precursor of unloading (DE), and plastic unloading front (EF).

Shock tests were performed with M-2 copper, D-16 aluminum alloy, beryllium, 38KhN3MFA steel, 02N18K9M5 maraging steel, and KhN75BMYu alloy. The velocity profiles of the free surface $U_{\text{f.s.}}(t)$ and the root-mean-square deviation of the particle velocity $D(t)$ were obtained in the experiments. The dependences of U_A and W on the projectile velocity U_{pr} were also constructed (Figs. 3–7).

2. Discussion of Results. At the macroscopic scale, the shape of the leading edge and the duration of individual sectors of the compression pulse characterize the dynamics of events proceeding at the microscale at the time of shock-wave transiting. The quantitative characteristic of the macroscopic response of the medium to shock loading is the space-time profile of the wave $U_{\text{f.s.}}(t)$ normally registered in shock tests of flat targets under uniaxial strain. The quantitative characteristic of fluctuating processes at the microscale is the temperature as a measure of intensity of random atomic motion. At higher scales, in particular, at the mesoscale, the quantitative characteristic of fluctuating properties of the medium is the dispersion of particle velocity. It has been established that the character of velocity dispersion in the process of shock loading depends on wave steadiness or unsteadiness. It has been shown experimentally and theoretically that dispersion in steady waves reaches the maximum value in the middle of the wave front and tends to zero when approaching the front apex [5]. It is seen in Fig. 2 that the slope of the loading front drastically decreases when the velocity dispersion vanishes, which indicates a change in the mechanism of stress relaxation. Starting from this moment, relaxation is performed due to another mechanism, which is switched not instantaneously but during a transitional stage (sector AB). After the transitional stage, the stress increases again but with a different rate. In fact, the transition to a new regime of dynamic deformation can be considered as a structural phase transition initiated by shock loading.

The mean velocity U_A (or normal stress) corresponding to the beginning of the transitional stage determines the dynamic threshold of the structural transition, which can be reversible or irreversible, depending on the strain rate. Figure 3 shows the free-surface velocity corresponding to this threshold versus the projectile velocity $U_A(U_{\text{pr}})$ for polycrystalline beryllium. For $U_{\text{pr}} = 120$ m/sec, the dependence $U_A(U_{\text{pr}})$ has an inflection after which the slope of the curve significantly decreases. Figure 3 also shows the spalling velocity as a function of the projectile velocity $W(U_{\text{pr}})$. Spalling fracture of the material starts at the projectile velocity corresponding to the inflection on the dependence $U_A(U_{\text{pr}})$. This means that irreversible changes occur in the material at $U_{\text{pr}} = 120$ m/sec in the course of the structural transition, which results in a change in material resistance to shock loading. The curve NN' is drawn through the point corresponding to the projectile velocity at which the strain gradient in the compression wave reaches the critical value, and the structural transition becomes irreversible. The free-surface velocity corresponding to the structural transition is denoted by U_{inst}.

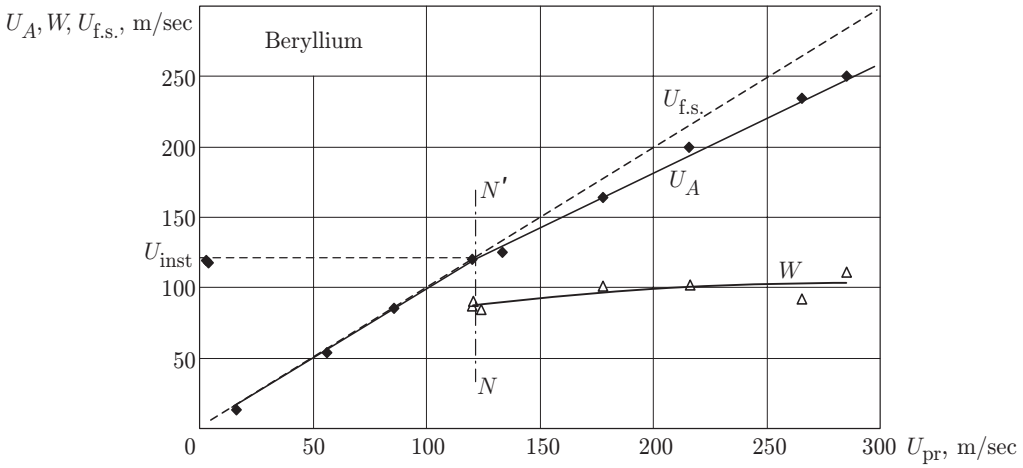

Fig. 3

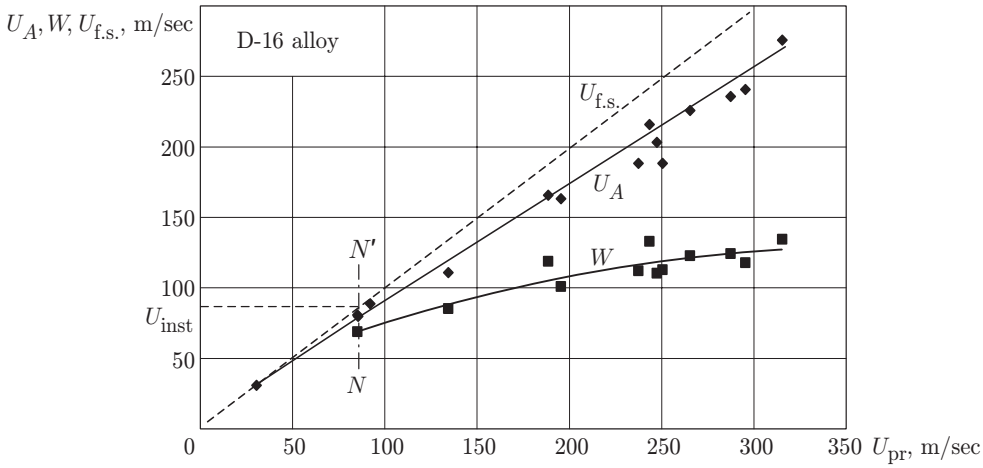

Fig. 4

The possibility of existence of irreversible structural transitions was considered theoretically in [6]. The microfracture model based on solving the nonlinear sine Helmholtz equation predicts unstable behavior of the crystalline lattice subjected to shear strain in the nonlinear-elastic range of loading. This instability leads to nucleation of large-scale structures, such as mesorotations, localized shear bands, vortex structures, and their combinations. These large-scale structures arise far before the transition to macroscopic plasticity. If the strain gradient does not exceed a certain critical value, these structures can disappear, i.e., the structural transition described above is still reversible at this stage. At higher strain gradients, a bifurcation transition from elasticity to plasticity is observed, which yields mesoscopic structures encountered in microstructural studies.

Structural transitions during dynamic compression are observed for all materials considered in the present work. Figure 4 also shows the inflection on the curve $U_A(U_{\text{pr}})$, which corresponds to the beginning of spalling fracture [see the dependence $W(U_{\text{pr}})$].

For plastic materials, such as copper, viscous high-strength steels, maraging steels, etc., the inflection on the curve $U_A(U_{\text{pr}})$ corresponds to the change in the character of the dependence of spalling velocity on the projectile velocity $W(U_{\text{pr}})$. This follows from the dependences $U_A(U_{\text{pr}})$ and $W(U_{\text{pr}})$ plotted in Figs. 4–7, which were obtained for the materials listed above. The inflections on the curves $U_A(U_{\text{pr}})$ and $W(U_{\text{pr}})$ correspond to one projectile velocity. The higher the threshold of material instability to compression U_{inst}, the higher its spalling strength.

To verify this statement, two lots of 38KhN3MFA high-strength steel were tested. One of these lots was tested in the state it was delivered, and the other was subjected to standard high-temperature treatment with quenching and medium tempering. The test results are shown in Figs. 8 and 9. Structural instability is observed at $U_{\text{pr}} = 200$ m/sec for the first lot of steel (Fig. 8) and at $U_{\text{pr}} = 263$ m/sec for the second lot. The threshold

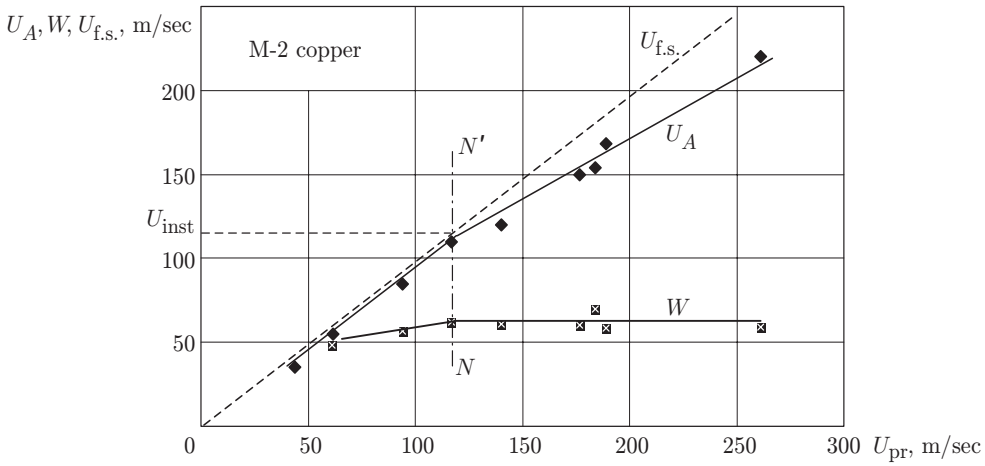

Fig. 5

velocity of structural instability is $U_{\text{inst}} = 159$ m/sec for the first lot of steel and $U_{\text{inst}} = 232.7$ m/sec for the second one. Accordingly, the spalling velocity varies from 159 to 180 m/sec for the first lot of steel (the mean velocity is 169.5 m/sec) and from 180.7 to 203.3 m/sec for the second lot (the mean velocity is 192 m/sec). Thus, spalling strength of the material correlates with the threshold of dynamic instability in compression U_{inst}. The results obtained indicate that experiments on spalling fracture under uniaxial loading of flat targets do not provide objective information on the value of dynamic strength of the material in tension in the microsecond range of loading duration.

3. Structural Instability of a Material and Resistance to High-Velocity Penetration. The normal stress at which an irreversible structural transition at the leading edge of the compression pulse occurs under uniaxial strain should be considered as an independent strength characteristic of a material, which determines the threshold of dynamic stability of the material to dynamic compression. Allowance for this characteristic is important not only for the development of theoretical models of uniaxial deformation but also for calculating high-velocity penetration parameters. The penetration depth of long-rod projectiles into a semi-infinite target is known to be determined by a modified Bernoulli equation, which was called the Alekseevskii–Tate equation [7, 8]:

$$Y + \rho_{\text{pr}}(U_{\text{pr}} - U_{\text{t}})^2/2 = \rho_{\text{t}} U_{\text{t}}^2/2 + R.$$

Here U_{t} is the mass velocity in the target material directly ahead of the projectile; Y and R are empirical constants determining dynamic strength of the projectile and target materials, respectively. The value of R determines the difference in behavior of the target material from an ideal incompressible fluid. The deformation micromechanisms determining the value of R are the object of current research in microplasticity. In known papers on penetration of high-velocity long-rod projectiles, it is argued that the physical meaning of the parameters R and Y remains still unclear [7, 8]. In some papers, the quantity R is identified with dynamic hardness of the material H_D, which is related to the dynamic yield point Y_D by the correlation dependence [9]

$$H_D = (3\text{–}3.5)Y_D. \tag{1}$$

In turn, the dynamic yield point is determined by the Hugoniot yield point σ_h:

$$Y_D = \sigma_h(1 - 2\nu)/(1 - \nu) \tag{2}$$

(ν is Poisson's ratio).

An analysis of the common features of the high-velocity penetration process and experimental results shows that the strength characteristic of resistance to penetration for targets of plastic (metals) and brittle (ceramics) materials is determined both by inertial forces and by resistance to plastic strain. This means that the strength component of resistance to penetration changes if the character of plastic deformation changes, for instance, because of the changes in the structural deformation mechanism.

Experiments on high-velocity penetration of projectiles into the target do not give information on the change in the mechanism of plastic deformation. At the same time, an analysis of wave processes shows that conditions of uniaxial strain are formed in the nose part of the projectile, at the so-called stagnation point (critical point of

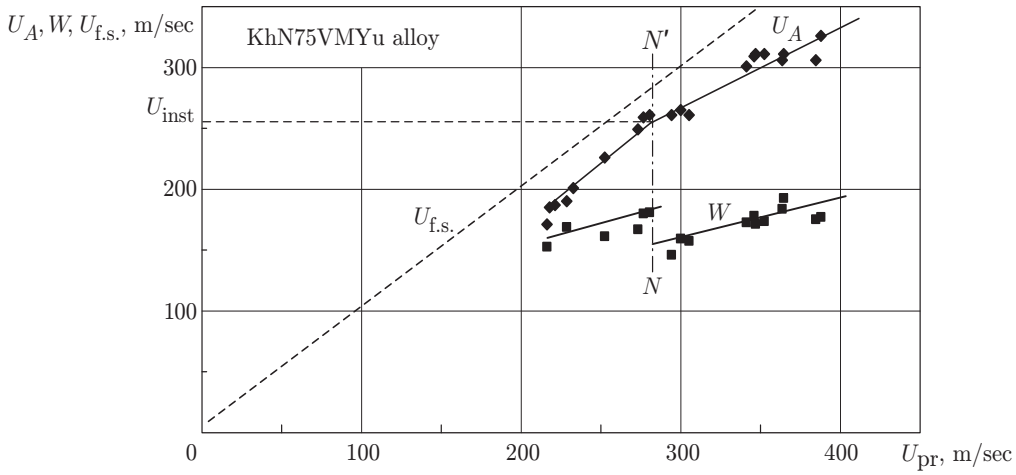

Fig. 6

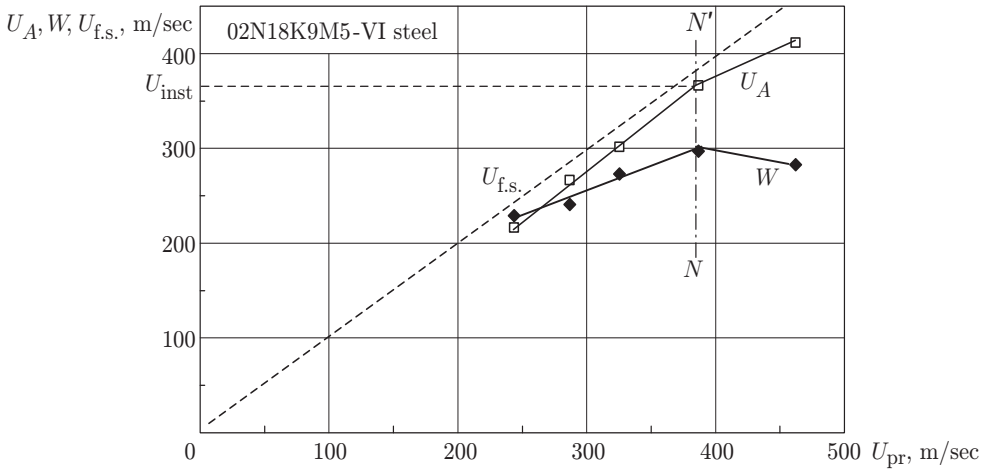

Fig. 7

TABLE 2

Target material	σ_h, GPa	R, GPa	C_{pl}, mm/μsec	U_{inst}, m/sec	σ_i, GPa
Aluminum D-16	0,35	0.6–0.7	5.35	80	0.58
Steel 38KhN3MFA	1,65	2.80–3.29	5.00	159	3.12
Maraging steel 02N18K9M5-VI	4.10	7.0–8.2	5.05	383	7.39
Titanium alloy VT-6	2.88	4.90–5.75	5.30	440	5.17

the flows on the target near the projectile) [8]. In contrast to tests on high-velocity penetration, shock testing of materials under uniaxial strain is rather informative. This allows one to use the test results for planar impact to determine the strength characteristic of the target material R; as this characteristic, we can use the stress σ_i corresponding to the loss of dynamic stability in compression:

$$\sigma_i = \rho_{\text{t}} C_{\text{pl}} U_{\text{inst}}/2. \tag{3}$$

Here C_{pl} is the velocity of the plastic front in tests under uniaxial strain.

Table 2 contains the values of R calculated by formulas (1) and (2) and the parameter σ_i calculated by formula (3) for a number of structural materials tested under uniaxial strain. The values of stress on the elastic precursor σ_h were obtained in tests on uniaxial deformation. It follows from Table 2 that the values of R determined

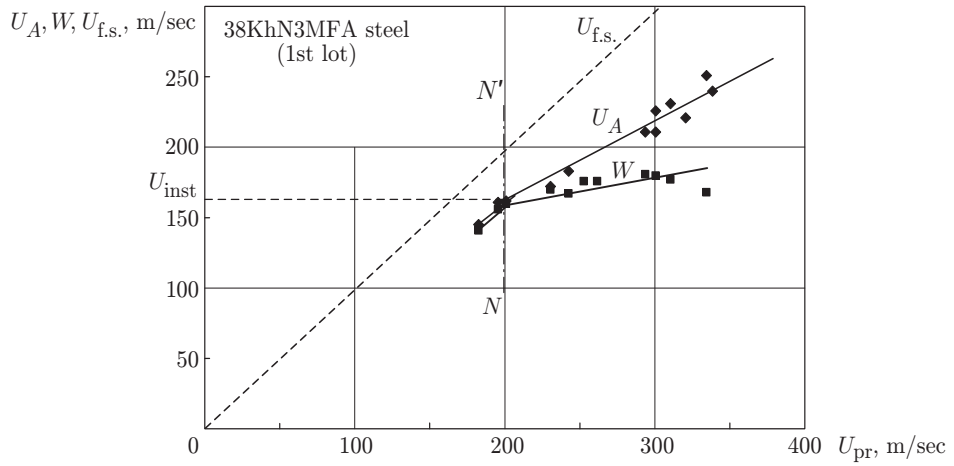

Fig. 8

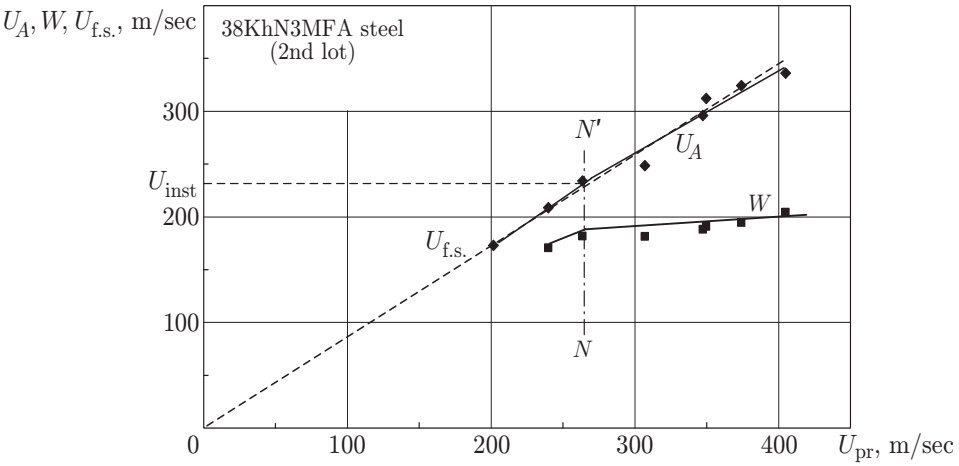

Fig. 9

by Tate's technique and the values of the threshold of dynamic stability in compression under uniaxial strain σ_i coincide for each material under study. This indicates that the strength characteristic of resistance to penetration R has a certain physical meaning. Its value is determined by the threshold of material instability in dynamic compression under conditions of uniaxial strain.

In the case of steady plastic waves, material instability under shock compression is initiated at a strain rate such that the dispersion of mass velocity at mesoscale 1 as a method of relaxation of internal stresses is absent. At this moment, relaxation at a higher scale, the so-called mesoscale 2, is initiated [3, 4]. Excitation of mesoscale 2 in a viscous material can also occur at a mass velocity below the threshold of the structural transition U_A. To clarify the latter statement, the time evolution of the free-surface velocity for a viscous material (Armco iron) and for a brittle material (beryllium) is shown in Fig. 10a and b. These velocities were measured by a high-velocity interferometer. The profile in Fig. 10a has an obviously oscillating character, whereas the profile in Fig. 10b is smooth. Since the transverse size of the interferometer laser beam coincides with the size of the structural element at mesoscale 2 (100–500 μm), velocity oscillations on the profile for Armco iron correspond to the motion of the structural element as a whole at mesoscale 2 and characterize relaxation of the structure at this scale. The dependence $U_{\text{f.s.}}(t)$ for beryllium is in line with the character of dispersion shown in Fig. 1b; a similar dependence for Armco iron corresponds to the character of dispersion shown in Fig. 1a. In a brittle material below the threshold of structural instability, mesoscale 2 is "frozen," and relaxation of internal stresses occurs only due to mobility of structural elements at

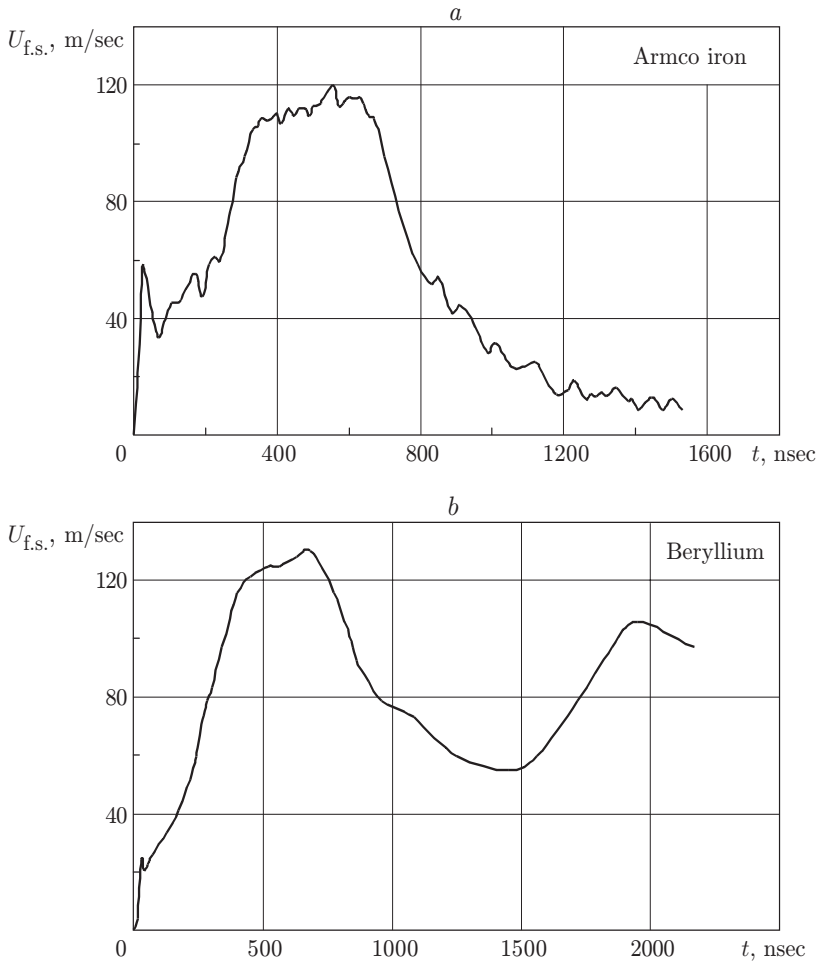

Fig. 10

mesoscale 1. When the relaxation capabilities of the material at mesoscale 1 are exhausted, internal stresses grow to a value at which relaxation at mesoscale 2 is initiated. In a viscous material, such as Armco iron, excitation of mesoscale 2 begins almost immediately after the elastic precursor, and relaxation of internal stresses in this material occurs simultaneously at two structural scales.

The length of the transitional zone AB (see Fig. 2) determines the scale of the structure at mesoscale 2. In particular, the length of the transitional zone for the profile shown in Fig. 2 is 100 nsec. In steel with a plastic-front velocity of 5 mm/μsec, the length of the transitional zone is $d_{\text{ms2}} = 500$ μm, which corresponds to mesoscale 2.

4. Conclusions. An analysis of the wave front under uniaxial strain and the process of spalling fracture of flat targets shows that experiments on spalling fracture do not provide objective information on the value of dynamic strength of a material in tension in the microsecond range of loading duration. Spalling strength of a material significantly depends on whether irreversible loss of structural stability of the material at the compression-pulse front occurs.

The threshold of structural instability of a material under shock compression under conditions of uniaxial strain determines the strength characteristic of target resistance to high-velocity penetration of long-rod projectiles.

This work was supported by the Federal Target Program of the Ministry of Industry and Science of the Russian Federation (Grant No. 40.010.11.1195).

REFERENCES

1. B. P. Glushak, V. F. Kuropatenko, and S. A. Novikov, *Investigation of Material Strength under Dynamic Loading* [in Russian], Nauka, Novosibirsk (1992).
2. Yu. I. Mescheryakov and A. K. Divakov, "Multiscale kinetics of microstructure and strain-rate dependence of materials," *Dymat J.*, No. 1, 271–287 (1994).
3. V. E. Panin, Yu. V. Grinyaev, and V. I. Danilov, *Structural Scales of Plastic Deformation and Fracture* [in Russian], Nauka, Novosibirsk (1990).
4. V. I. Vladimirov, V. N. Ivanov, and N. D. Priemskii, "Mesoscopic scale of plastic deformation," in: *Physics of Strength and Plasticity* [in Russian], Nauka, Leningrad (1986), pp. 69–79.
5. T. A. Khantuleeva and Yu. I. Mescheryakov, "Kinetics and nonlocal hydrodynamics of mesostructure formation in dynamically loaded media," *Fiz. Mezomekh.*, **2**, No. 5, 5–17 (1999).
6. É. L. Aéro, "Microscale deformations in two-dimensional lattice structural transitions under critical shear," *Fiz. Tverd. Tela*, **42**, No. 6, 1147–1153 (2000).
7. V. B. Lazarev, A. S. Balankin, A. D. Izotov, and A. A. Kozhushko, *Structural Stability and Dynamic Strength of Inorganic Materials* [in Russian], Nauka, Moscow (1993).
8. V. Hohler and A. J. Stilp, "Long-rod penetration mechanics," in: *High Velocity Impact Dynamics*, John Wiley and Sons, New York (1990), pp. 321–404.
9. A. Tate, "A theory for the deceleration of long rods after impact," *J. Mech. Phys. Solids*, **15**, No. 6, 387–399 (1967).